"Hedgehog Ball"-Shaped Nanoprobes for Multimodal Detection and Imaging of Inflammatory Markers in Osteosarcoma Using Fluorescence and Electrochemiluminescence

Chen Zhao, Mo Ma, Jukun Yang, Zhuoxin Ye, Pinyi Ma,* and Daqian Song*

Read Online

ACCESS | Metrics & More | Article Recommendations | SI Supporting Information

ABSTRACT: Inflammation can affect the progression of cancer at tumor sites, such as in osteosarcoma, by intensifying metastasis and complicating outcomes. The current diagnostic methods lack the specificity and sensitivity required for early and accurate detection, particularly in differentiating between inflammation-induced changes and tumor activities. To address this, a novel "hedgehog ball"-shaped nanoprobe, Fe_3O_4@Au-pep-CQDs, was developed and designed to enhance the detection of caspase-1, a key marker of inflammation. This magnetic nanoprobe facilitates simultaneous fluorescence (FL) and electrochemiluminescence (ECL) detection. Magnetic separation minimizes the quenching of nanoparticles in solution and eliminates the need for frequent electrode replacement in ECL tests, thereby simplifying diagnostic procedures. The experimental results showed that in the detection of caspase-1, the nanoprobe had a detection limit of 0.029 U/mL (FL) and 0.033 U/mL (ECL) and had a dynamic range of 0.05 to 1.0 U/mL. Additionally, the nanoprobe achieved high recovery rates of 94.36 to 102.44% (FL) and 94.36−100.12% (ECL) in spiked biological samples. Furthermore, the nanoprobe's capabilities were extended to in vivo bioimaging to provide direct, intuitive visualization of biological processes. These novel nanoprobes were able to significantly enhance the accurate detection of inflammation at tumor sites, thereby optimizing both diagnostic and therapeutic strategies.
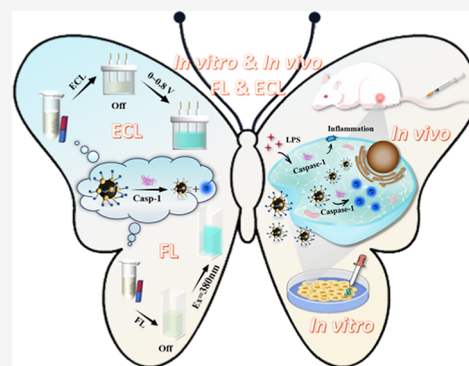
INTRODUCTION

Inflammation at tumor sites can significantly influence the progression of cancer by exacerbating metastasis and invasion processes.[1,2] Particularly in malignant tumors such as osteosarcoma, which are inherently prone to hematogenous spread, the presence of an inflammatory microenvironment can dramatically accelerate disease progression.[3,4] Clinical studies have corroborated that malignant tumors frequently exhibit inflammation, while benign tumors generally do not.[5,6] This inflammation is not merely a byproduct but a catalyst that promotes tumor growth, invasion, and metastasis, thereby complicating treatment and worsening patient outcomes.[7,8] The diagnosis and monitoring of such tumors face significant challenges due to the complexity and cost of the current detection methods.

Caspase-1 plays a key role in the inflammatory response and is an important indicator of inflammation.[9,10] Moreover, the current methods are often cumbersome, costly, and lack the specificity and sensitivity required for early and accurate diagnosis. Existing probes, such as those targeting caspase-3 and caspase-9, are effective for evaluating apoptosis during post-treatment monitoring; however, they cannot provide reliable metrics for assessing the severity of cancer.[11−14] This gap in diagnostic capabilities highlights the urgent need for novel detection methods that can directly correlate with the

inflammatory markers at tumor sites or offer a clearer picture of the tumor's biological status and its potential response to therapies.

Addressing these challenges, we developed a novel, cost-effective magnetic nanoprobe named Fe_3O_4@Au-pep-CQDs nanoprobe, which had a distinctive "hedgehog ball" shape for multimodal detection. This design involved the integration of gold nanoparticles, grown in situ on Fe_3O_4 nanoparticles, with carbon quantum dots (CQDs) that have exceptional electrochemical and fluorescent properties (Scheme 1A). The Fe_3O_4@Au nanoparticles were connected to CQDs via peptide chains that can be recognized specifically by caspase-1. Upon the interaction with caspase-1, the specific peptide sequence-YVAD-is cleaved,[15] resulting in the release of CQDs from the vicinity of Fe_3O_4@Au nanoparticles. Magnets were subsequently applied to effectively isolate the cleaved Fe_3O_4@Au nanoparticles and unreacted Fe_3O_4@Au-pep-CQDs nanoprobe from the solution, leaving only the liberated CQDs. This

Scheme 1. Schematic Representation of the Synthesis, Detection Mechanisms, and Intracellular Activity of Fe$_3$O$_4$@Au-pep-CQDs Nanoprobe. (A) The Step-by-Step Synthesis of Fe$_3$O$_4$@Au-pep-CQDs Nanoprobe. (B) The Dual-Modality Detection Using FL and ECL of the Nanoprobes. (C) The Mechanism of Action of the Nanoprobes Within a Cellular Environment
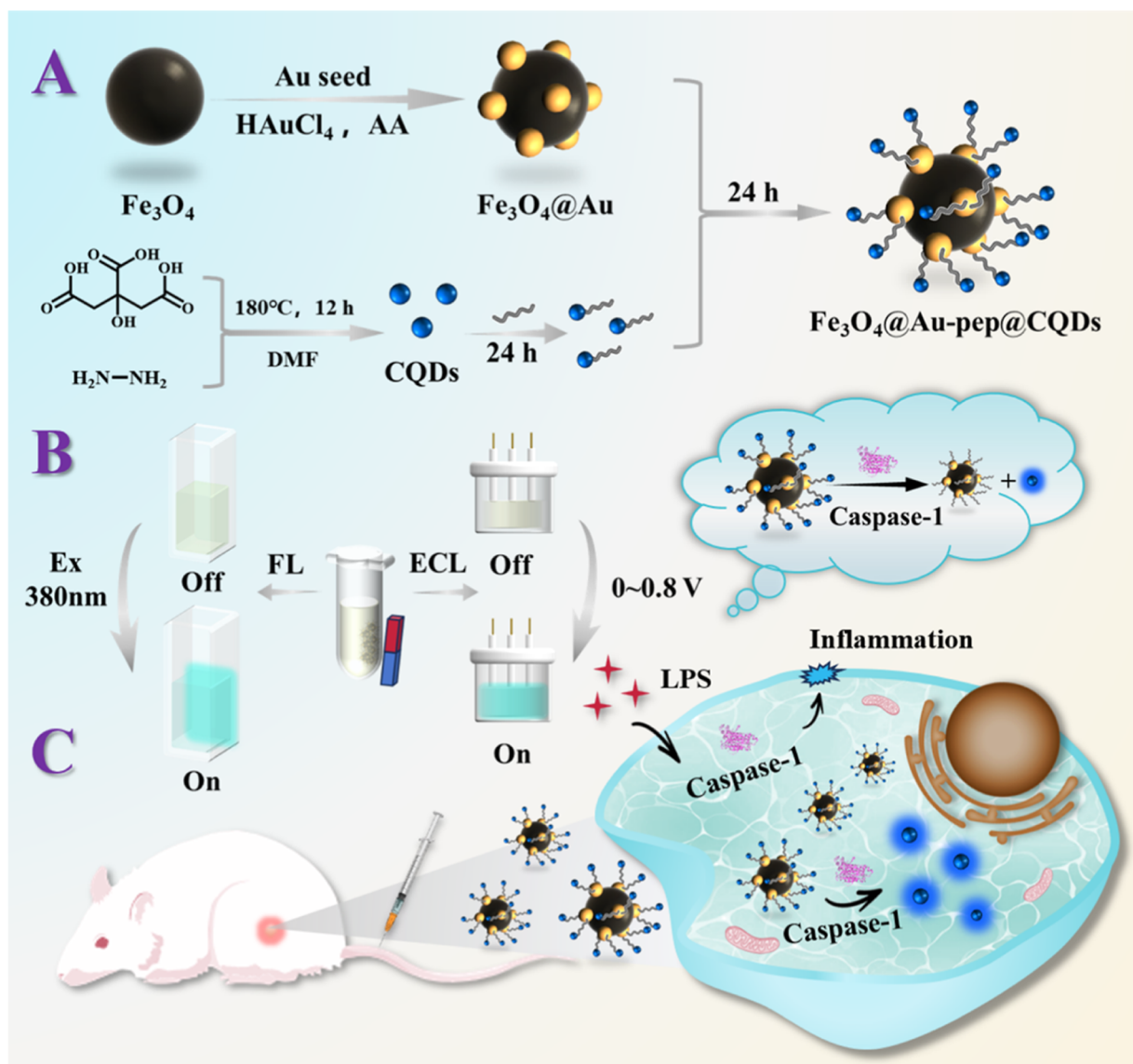
process of magnetic separation not only eliminates the influence of Förster resonance energy transfer (FRET)[16] and inner filter effects (IFE)[17] on the fluorescence (FL) of CQDs but also ensures that the electrochemiluminescence (ECL) measurements of CQDs are free from interference by other substances (Scheme 1B). The concentration of CQDs in the test solution was found to be positively correlated with the caspase-1 concentration, resulting in a concurrent increase in both FL and ECL signals. Additionally, the prepared test solution could undergo FL and ECL detection either independently or in combination and was unaffected by the sequence of testing. The nanoprobe's ability to perform both detection modes simultaneously not only enhances the accuracy and reliability of the results but also optimizes operational efficiency by reducing the time and costs associated with the experimental procedures. Furthermore, with the magnetic targeting capabilities of the nanoprobes, we selected osteosarcoma as the primary biological model to evaluate

caspase-1 and explored their potential for fluorescence imaging of organisms (Scheme 1C).

■ EXPERIMENTAL PROCEDURE

Synthesis of CQDs. CQDs were synthesized using a modified solvothermal method.[18] Initially, 2.1 g of citric acid was dissolved in 10 mL of DMF while stirring. Subsequently, 1.0 mL of hydrazine hydrate was added dropwise to the solution. The mixture was then transferred to an autoclave and subjected to a solvothermal reaction at 180 °C for 12 h. After cooling to room temperature, the resultant brown solution was centrifuged at 12,000 rpm for 10 min to remove large particulate residues. The supernatant was dialyzed against deionized water using a 1000 Da dialysis bag to purify the CQDs. Finally, the purified CQDs were stored in a sealed container at 4 °C for subsequent experiments.

Synthesis of Fe$_3$O$_4$@Au Nanoparticles. *Preparation of Gold Seeds.* Gold seeds of approximately 4 nm in size[19] were prepared by adding 20 mL of 5 mM HAuCl$_4$ solution to 360
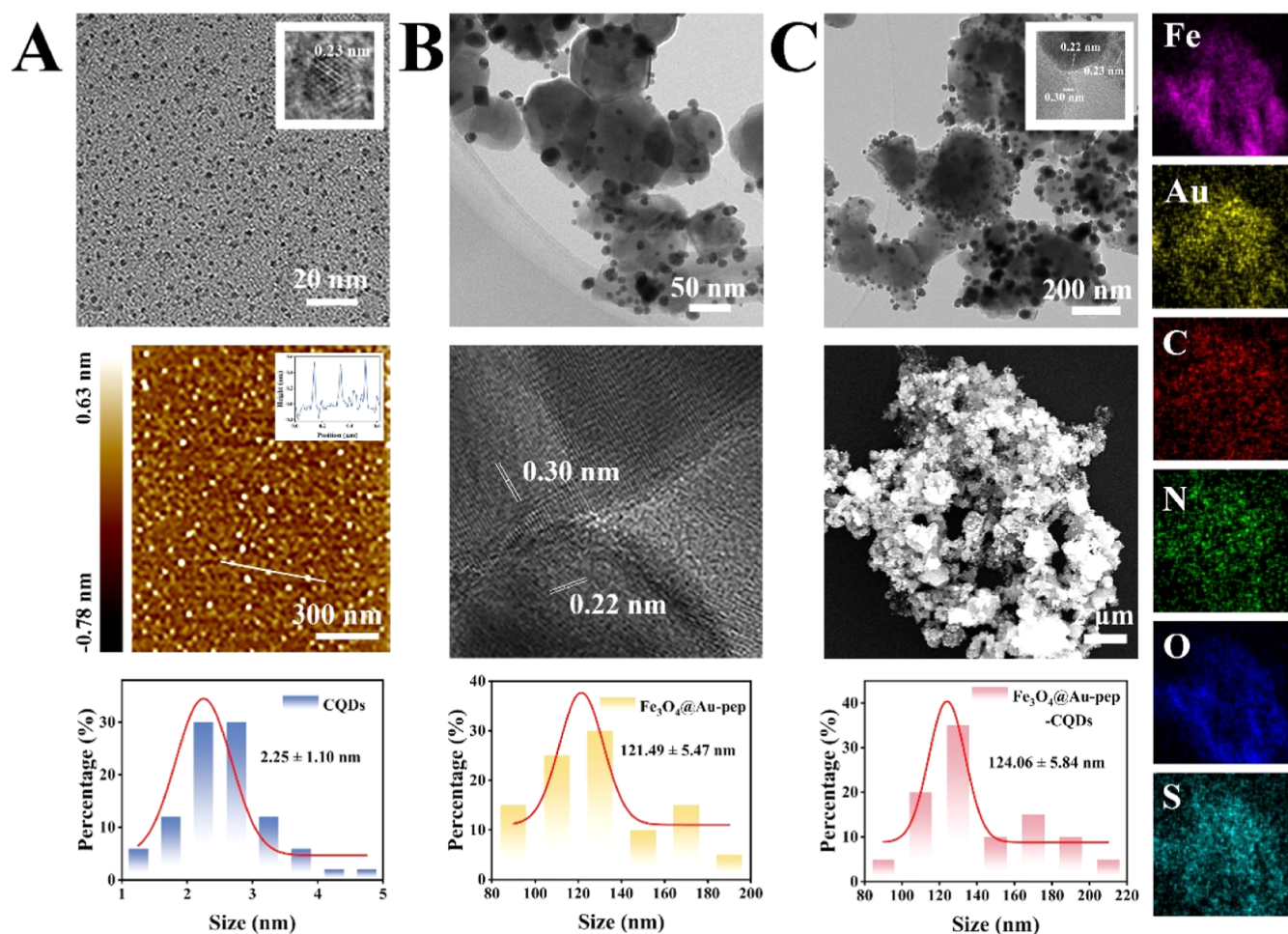
Figure 1. (A) TEM, HRTEM and AFM images, and particle size distribution of CQDs. (B) TEM and HRTEM images, and particle size distribution of Fe_3O_4@Au nanoparticles. (C) TEM, HRTEM and EDC images, and particle size distribution of Fe_3O_4@Au-pep-CQDs nanoprobe.

mL of deionized water, followed by the addition of 20 mL of 5 mM sodium citrate solution. The mixture was vigorously stirred, and 10 mL of freshly prepared 0.1 M $NaBH_4$ solution was then quickly added. The addition resulted in an immediate color change to orange-red. The mixture was stirred continuously for 4 h at room temperature and then stored at 4 °C.

Magnetic Nanoparticle Formation. 45 mg of Fe_3O_4 nanoparticles were dispersed in 300 mL of 1% (v/v) APTES in ethanol and mechanically stirred for 24 h to allow for amino modification. The particles were magnetically separated, washed thrice with water, and redispersed in 100 mL of the previously prepared gold seed solution. This suspension was stirred for 5 h, and the particles were magnetically reseparated. The particles were then sequentially treated with 4 mL of 1% $HAuCl_4$, 12 mL of 10% ammonium hydroxide, and 32 mL of 10 mM ascorbic acid; each was added dropwise while shaking for 4.5 h. Following the completion of the reaction, a magnet was used to isolate the solids, which were then alternately washed with water and ethanol twice. The final product was redispersed in ultrapure water to prepare a 1 mg/mL Fe_3O_4@Au nanoparticles solution, which was then stored at 4 °C.[20]

Synthesis of Fe_3O_4@Au-pep-CQDs Nanoprobe. *Conjugation of Peptides to CQDs.* Initially, 1 mL of the previously synthesized CQDs solution was mixed with 1 mL of MES buffer (10 mM, pH 6.0). To this mixture, 200 μL of EDC solution (5 mg/mL) and 200 μL of NHS solution (9.5 mg/ mL) were added, and the solution was stirred for 1 h. After the pH was adjusted to 7.4, 5 μL of peptide chain GRTYVA-DYTTLPATC (2 mg/mL) was added. The mixture was stirred thoroughly and allowed to react overnight. Subsequently, the product was dialyzed against deionized water using a 2000 Da dialysis bag for 1 day to remove unreacted components.[21]

Assembly of Fe_3O_4@Au-pep-CQDs Nanoprobe. 10 μL of TCEP solution (1 mg/mL) was added to the peptide-conjugated CQDs and stirred vigorously for 2 min. Then, 2 mL of the previously prepared Fe_3O_4@Au nanoparticles (1 mg/mL) was added, and the mixture was shaken vigorously. Next, 2 mL of NaCl solution (40 mg/mL) was added dropwise, and the mixture was shaken overnight to ensure complete reaction. The solids were then separated via magnetic separation, washed three times with water to remove impurity, and finally redispersed in 2 mL of deionized water. The prepared Fe_3O_4@Au-pep-CQDs nanoprobe was stored at 4 °C until further use.

Fluorescence and ECL Detection of Caspase-1 In Vitro Using Fe_3O_4@Au-pep-CQDs Nanoprobe. A 0.1 mg/ mL solution of Fe_3O_4@Au-pep-CQDs nanoprobe was prepared in phosphate-buffered saline (PBS). The solution was mixed with caspase-1 and incubated at 37 °C with oscillation. After incubation, magnetic separation was used to isolate the nanoparticles, and the supernatant was collected for
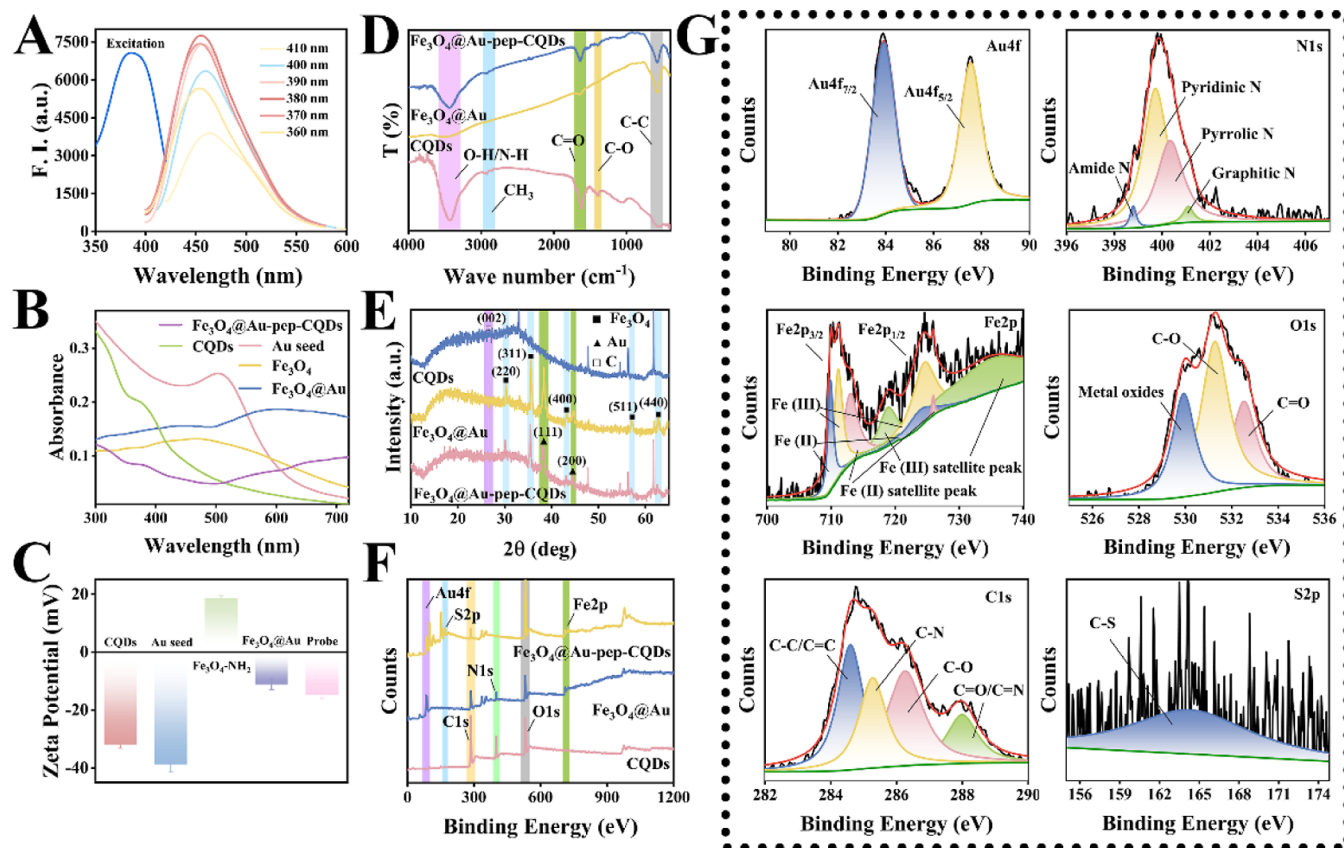
Figure 2. (A) Optimal excitation wavelengths of CQDs and their fluorescence emission spectra at different excitation wavelengths. (B) UV−vis absorption spectra of CQDs, Au seed, Fe_3O_4 nanoparticles, Fe_3O_4@Au nanoparticles and Fe_3O_4@Au-pep-CQDs nanoprobe. (C) Zeta potential changes of CQDs, Au seed, Fe_3O_4−NH_2, Fe_3O_4@Au nanoparticles and Fe_3O_4@Au-pep-CQDs nanoprobe. (D) FT-IR spectra of CQDs, Fe_3O_4@Au nanoparticles and Fe_3O_4@Au-pep-CQDs nanoprobe. (E) XRD patterns of CQDs, Fe_3O_4@Au nanoparticles and Fe_3O_4@Au-pep-CQDs nanoprobe. (F) XPS spectra of CQDs, Fe_3O_4@Au nanoparticles and Fe_3O_4@Au-pep-CQDs nanoprobe. (G) Detailed peaks of Au, Fe, C, N, O and S elements in the XPS spectrum of Fe_3O_4@Au-pep-CQDs nanoprobe.

analysis. Fluorescence spectra of the supernatant were measured at an excitation wavelength of 380 nm. For ECL detection, in which the ECL spectra were recorded, the supernatant was diluted 2-fold in PBS (10 mM) and analyzed by cyclic voltammetry at voltages between 0 and 0.8 V and a scan rate of 300 mV/s.

■ RESULTS AND DISCUSSION

Preparation and Characterization of Fe_3O_4@Au-pep-CQDs Nanoprobe. The nanoprobes were composed of carboxyl-modified CQDs linked to Fe_3O_4@Au nanoparticles via peptide chains. The CQDs, synthesized using the established methods, were analyzed by TEM and HRTEM. These analyses revealed that the CQDs had an average particle size of approximately 2.25 ± 1.10 nm and a thickness of about 0.6 nm confirmed by AFM (Figure 1A), which is consistent with the thickness of a single graphite layer.[22] Further characterization of Fe_3O_4@Au nanoparticles via TEM showed that the particles had a particle size of 121.49 ± 5.47 nm. The lattice spacings of gold and iron were determined by HRTEM and found to be 0.22 and 0.30 nm, respectively (Figure 1B), which align with the values reported in the literature.[23,24] The overall nanoprobe size measured by TEM was 124.06 ± 5.84 nm. EDS confirmed the successful preparation of the nanoparticles, showing that elements were properly distributed (Figure 1C). Additionally, HRTEM analysis effectively verified that the CQDs were connected to Fe_3O_4@Au nanoparticles,

affirming the structural integrity and the successful synthesis of the nanoprobe.

Optical properties of the CQDs were examined across various excitation wavelengths, and the excitation wavelength of 380 nm and the emission wavelength of 456 nm were found to be the optimal wavelengths that resulted in the most effective fluorescence response (Figure 2A). Physical images of the CQDs under natural light and UV illumination (365 nm) are displayed in Figure S1A. The CIE chromaticity diagram of the CQDs at the optimal excitation wavelength is shown in Figure S1B. And Figure S1C is the schematic diagram of the structural formula of CQDs. The fluorescence lifetime of the CQDs was determined to be 408 ns, and the quantum yield was 3.92% (Figure S2). ECL properties were further characterized, showing that there were significant oxidation currents at 0.79 V, which closely matches the expected ECL excitation potential (0.8 V, Figures S3 and S4). The ECL efficiency was 1.52. UV−vis spectroscopy revealed changes in the absorption peaks, confirming that the Fe_3O_4@Au nanoparticles fraction was successfully synthesized (Figure 2B). The UV spectra of CQDs and Fe_3O_4@Au-pep-CQDs nanoprobe were analyzed comparatively, and both of them possessed absorption peaks at 380 nm, which showed that CQDs and Fe_3O_4@Au nanoparticles were successfully connected. Zeta potential measurements showed the expected charge properties: carboxyl-coated CQDs and gold seeds were negatively charged, whereas amino-coated Fe_3O_4 nanoparticles were
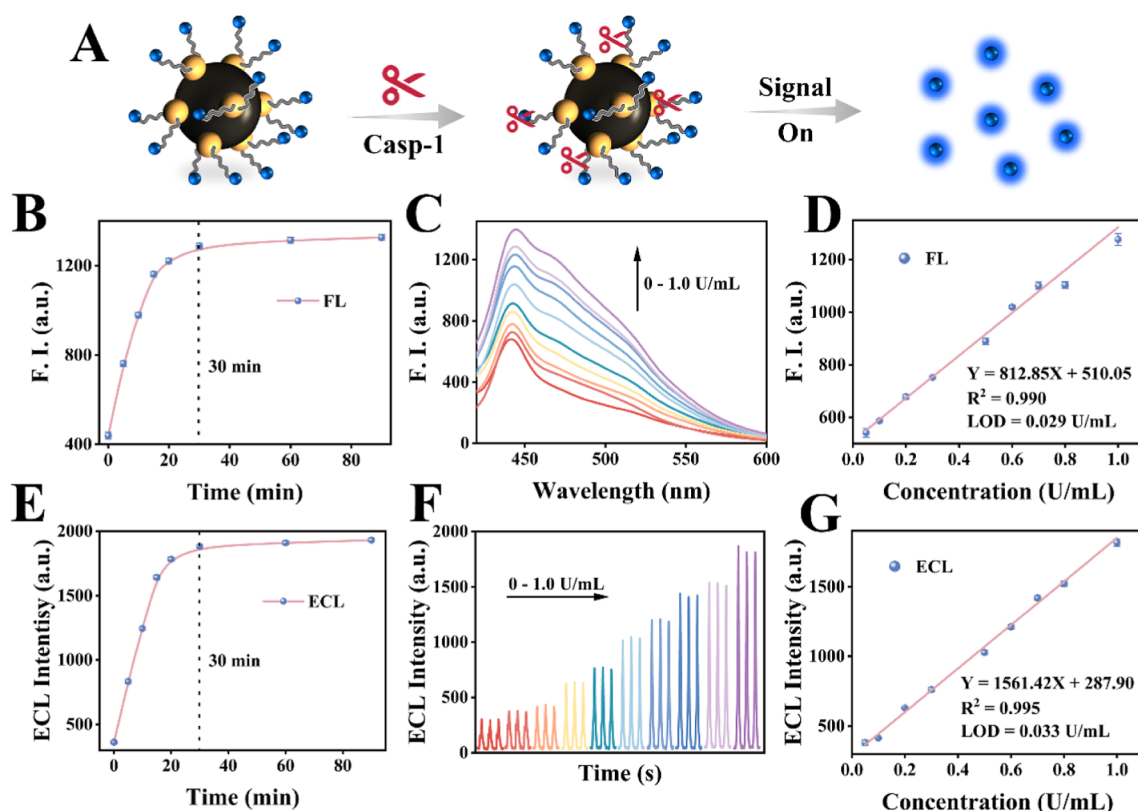
Figure 3. (A) Schematic representation of the reaction mechanism of Fe$_3$O$_4$@Au-pep-CQDs nanoprobe with caspase-1. (B) Time-dependent variation in FL intensity upon incubating 0.1 mg/mL Fe$_3$O$_4$@Au-pep-CQDs nanoprobe with caspase-1 (1.0 U/mL) at 37 °C and pH 7.4. (C) FL intensity of 0.1 mg/mL Fe$_3$O$_4$@Au-pep-CQDs nanoprobe incubated with human caspase-1 at different concentrations (0.05, 0.1, 0.2, 0.3, 0.5, 0.6, 0.7, 0.8, and 1.0 U/mL) at 37 °C and pH 7.4 for 30 min. (D) ECL linear response of Fe$_3$O$_4$@Au-pep-CQDs nanoprobe to the presence of caspase-1 at concentrations ranging from 0.05 to 1.0 U/mL (n = 3). (E) Time-dependent change in ECL intensity upon incubating 0.1 mg/mL Fe$_3$O$_4$@Au-pep-CQDs nanoprobe with caspase-1 (1.0 U/mL) at 37 °C and pH 7.4. (F) ECL intensity of 0.1 mg/mL Fe$_3$O$_4$@Au-pep-CQDs nanoprobe incubated with human caspase-1 at different concentrations (0.05, 0.1, 0.2, 0.3, 0.5, 0.6, 0.7, 0.8, and 1.0 U/mL) at 37 °C and pH 7.4 for 30 min. (G) FL linear response of Fe$_3$O$_4$@Au-pep-CQDs nanoprobe to caspase-1 at concentrations ranging from 0.05 to 1.0 U/mL (n = 3).

Table 1. Detection of Caspase-1 Activity in Extracts of MG-63 Cells With LPS-Induced Inflammation Using the Fe$_3$O$_4$@Au-pep-CQDs Nanoprobe

	endogenous caspase-1 (U/mL)	added (U/mL)	measured (U/mL)	recovery rate (%)	RSD (%) (n = 3)
FL	0.318	0.1	0.420 ± 0.022	102.19	5.27
		0.2	0.523 ± 0.023	102.44	4.35
		0.3	0.606 ± 0.022	96.01	3.61
		0.4	0.699 ± 0.017	95.23	2.47
		0.5	0.809 ± 0.025	98.17	3.06
ECL	0.305	0.1	0.399 ± 0.011	94.36	2.67
		0.2	0.501 ± 0.019	98.09	3.72
		0.3	0.593 ± 0.010	96.07	1.76
		0.4	0.702 ± 0.011	99.16	1.62
		0.5	0.806 ± 0.016	100.12	1.99

positively charged. The Fe$_3$O$_4$ nanoparticles adhered to gold seeds via electrostatic adsorption and Au−N bonding,[25,26] resulting in a composite structure with an enhanced negative charge on the Fe$_3$O$_4$@Au-pep-CQDs nanoprobe (Figure 2C).

The structural and compositional integrity of the nanoprobes was validated through FT-IR (Figure 2D), XRD (Figure 2E), and XPS analyses (Figures 2F,G, S5 and S6). The FT-IR analysis revealed the characteristic vibration peaks of O−H/N−H at 3440 cm^{-1}, C−H at 2930 cm^{-1}, C═O at 1630 cm^{-1},

C−O at 1380 cm^{-1}, and C−C at 590 cm^{-1}. These peaks indicate the presence of the expected functional groups. XRD analysis confirmed the crystal lattices corresponding to Fe$_3$O$_4$, Au, and CQDs, verifying the phase purity of the components.[27] XPS results further supported the nanoprobe's composition, with peaks corresponding to Au 4f and Fe 2p validating the successful synthesis of Fe$_3$O$_4$@Au nanoparticles, and peaks corresponding to S 2p confirming the successful assembly of Fe$_3$O$_4$@Au-pep-CQDs nanoprobe. These functional groups and elemental valence states confirm the successful synthesis of CQDs, Fe$_3$O$_4$@Au nanoparticles, and Fe$_3$O$_4$@Au-pep-CQDs nanoprobe. The stability of CQDs was determined through FL and ECL. The FL intensity of CQDs was not significantly changed for 10 consecutive days (Figure S7), and the stability of the CQDs based on ECL intensity after 10 consecutive scanning cycles was also high (Figure S8). This indicates that the CQDs are stable and ideally suited for both FL and ECL applications.

Response of Fe$_3$O$_4$@Au-pep-CQDs Nanoprobe to Caspase-1 In Vitro. First, optimization of the reaction time showed that the optimal duration for both analytical methods was 30 min (Figure 3B,E). This duration adequately allows the recognition of caspase-1 by the substrate nanoprobe. Subsequently, 0.1 mg/mL Fe$_3$O$_4$@Au-pep-CQDs nanoprobe was incubated with caspase-1 in PBS (1 mM, pH 7.4) at varying concentrations at 37 °C for 30 min while shaking.

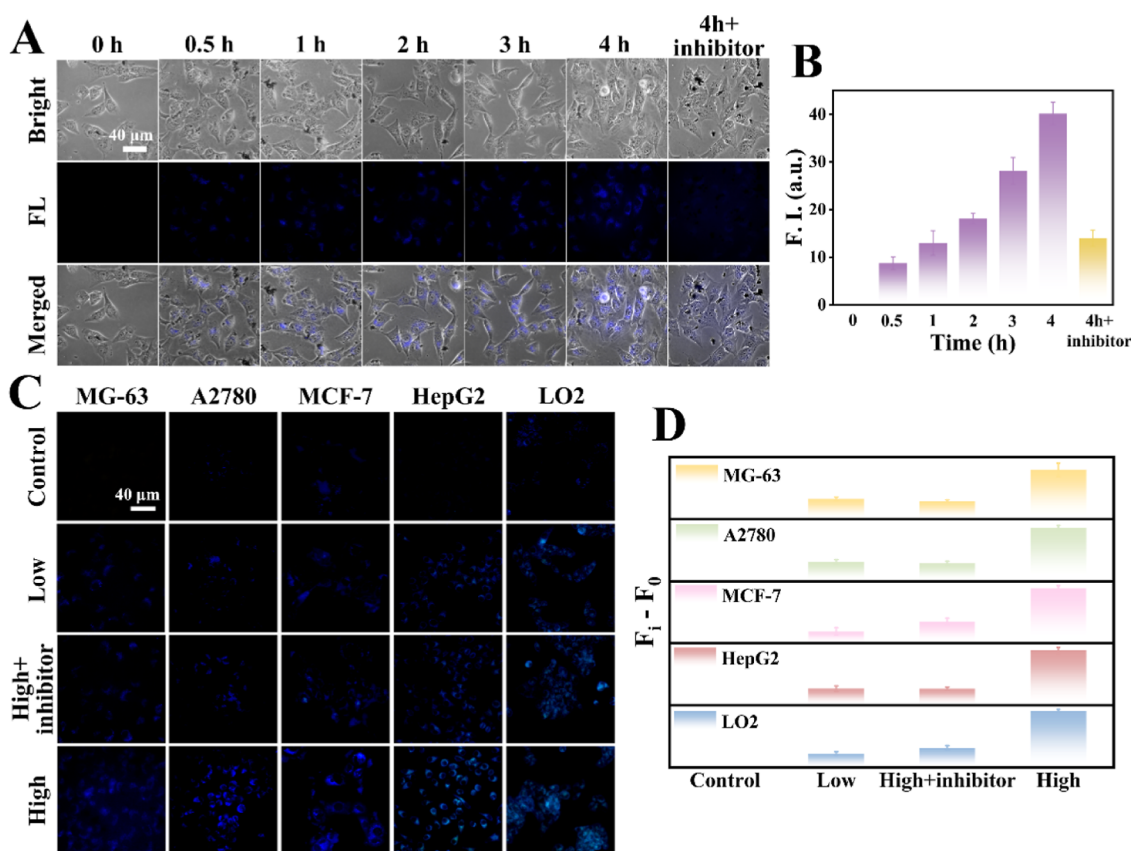**Figure 4.** (A) Fluorescence images of LPS-induced inflammation in MG-63 cells after incubating with Fe_3O_4@Au-pep-CQDs nanoprobe for different times, and fluorescence images of MG-63 cells captured after incubating with Fe_3O_4@Au-pep-CQDs nanoprobe + inhibitor for 4 h. (B) Analysis of fluorescence intensities of images in (A). (C) Versatility of Fe_3O_4@Au-pep-CQDs nanoprobe. (D) Analysis of fluorescence intensities of images in (C).

Following the magnetic separation of the samples, the supernatant was subjected to fluorescence intensity analysis. As depicted in Figure 3C, an increase in caspase-1 concentration led to enhanced fluorescence intensity. The corresponding linear relationship illustrated in Figure 3D showed a regression equation of $Y = 812.85X + 510.05$ over the range of 0.05 to 1.0 U/ml, with an R^2 value of 0.990 and a detection limit (LOD = $3\sigma/k$, σ is the standard deviation of 11 blank responses and k is the slope of the linear calibration curve) of 0.029 U/mL. Another portion of the supernatant was diluted with an equal volume of PBS (10 mM, pH = 7.4) and triethylamine (TEA) (0.5% v/v). The three-electrode system, consisting of an Ag/AgCl electrode (saturated KCl) as the reference electrode, a platinum wire electrode as the counter electrode and a modified glass carbon electrode (GCE, Φ = 4 mm) as the working electrode, was then directly inserted into the solution to measure the ECL signal. As illustrated in Figure 3F, the ECL intensity was proportional to the caspase-1 concentration. The corresponding linear relationship is detailed in Figure 3G, showing a regression equation of $Y = 1561.42X + 287.90$ across the concentration range of 0.05 to 1.0 U/ml, with an R^2 value of 0.995 and a detection limit (LOD = $3\sigma/k$, σ is the standard deviation of 11 blank responses and k is the slope of linear calibration curve) of 0.033 U/mL. Table S1 shows the comparison of detection results by Fe_3O_4@Au-pep-CQDs nanoprobe and those reported in the literature.

We evaluated the effect of pH on the FL and ECL signals of the CQDs and Fe_3O_4@Au-pep-CQDs nanoprobe. The results

indicated that the physiological conditions (pH = 7.4) were optimal conditions for these nanoprobes (Figure S9). Additionally, tests against various potential interferents, including Ca^{2+}, Mg^{2+}, BSA, GST, HAase, and caspase-3, demonstrated their minimal impacts on both FL and ECL signals, confirming that the Fe_3O_4@Au-pep-CQDs nanoprobe has high specificity and resistance to interference found in a physiological environment (Figure S10). Further examinations of the CQDs' response to different interferences such as Fe^{2+}, Fe^{3+}, Cu^{2+}, BSA, caspase-1, caspase-3, and lysate, revealed their robust anti-interference properties, showcasing their capability to resist to common biological substances (Figure S11). The addition of a specific inhibitor (Ac-YVAD-cmk) to the caspase-1 substrate also highlighted the nanoprobes' selectivity, affirming their ability to specifically target and detect caspase-1 (Figure S12).

In addition, we investigated the impact of magnetic separation on FL signal changes by comparing magnetically separated and nonseparated solutions (Figure S13). The results demonstrated that magnetic separation helped avoid FRET and IFE, thereby enhancing the fluorescence signal, reducing systematic errors, and improving the accuracy of nanoprobe detection. We also examined the effect of TEA addition on the fluorescence signal (Figure S14). The presence of TEA had no effect on fluorescence detection, and the fluorescence trends of the TEA-added group and control group were consistent. This confirms that the nanoprobe can effectively support both FL-ECL and ECL-FL detection in sequential orders, and the detection order has no influence on
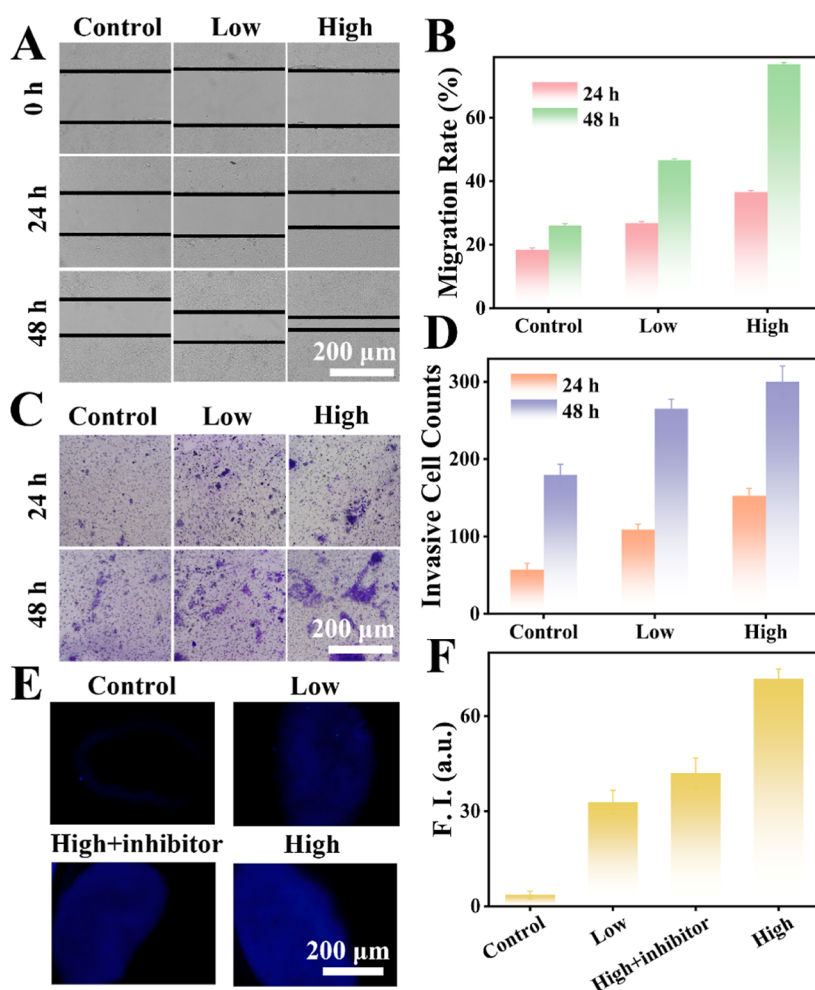
Figure 5. (A) Scratch experiments of cells incubated with blank control, 5 μg/mL LPS, and 20 μg/mL LPS. (B) Analysis of data in (A). (C) Transwell cell invasion assay of cells incubated with blank control, 5 μg/mL LPS, and 20 μg/mL LPS. (D) Analysis of data in (C). (E) 3D tumor cell model simulating the tumor inflammatory microenvironment developed using LPS induction, and the setup of the control group, LPS (20 μg/mL) + inhibitor group, LPS (5 μg/mL) group, and LPS (20 μg/mL) group. (F) Analysis of fluorescence intensities of images in (E).

the results. This feature is particularly beneficial when the sample volume is limited, as it eliminates the need to divide the sample for both FL and ECL tests. That is, one solution can be used for both tests, which can significantly reduce the need for large sample amounts.

In conclusion, this comprehensive evaluation underscores the excellent specificity and versatility of the Fe$_3$O$_4$@Au-pep-CQDs nanoprobe under various testing conditions, confirming their efficacy in accurately detecting caspase-1 in complex biological environments.

Detection of Real Samples by Fe$_3$O$_4$@Au-pep-CQDs Nanoprobe Through Spiked Recovery Experiments. Inflammation was induced in osteosarcoma MG-63 cells using lipopolysaccharide (LPS).[28] The inflamed MG-63 cells were subjected to three freeze–thaw cycles at −80 and 20 °C.[29] The resulting cell lysate was mixed with the Fe$_3$O$_4$@Au-pep-CQDs nanoprobe, and the measured signals are presented in Table 1. The recovery rates for caspase-1-spiked samples were 95.23−102.44% using the FL method and 94.36−100.12% using the ECL method. The numbers demonstrate the high accuracy and efficacy of the nanoprobes in detecting real biological samples. Moreover, both nanoprobe-based assays had excellent stability, as indicated by the low relative standard deviation values (<5.3%). The concentration of

caspase-1 in the cell lysate, measured using the caspase-1 activity assay kit, was 0.285 ± 0.026 U/mL, which closely matches the concentration detected by the nanoprobes. This finding highlights the practicality and reliability in the biological sample analysis of the probe.

Response and Imaging of Fe$_3$O$_4$@Au-pep-CQDs Nanoprobe in Cancer Cells. LPS is widely recognized as a potent inducer of inflammation and is known to activate the caspase-1 pathway and trigger inflammatory responses in cells.[30,31] In this study, MG-63 cells were cultured and treated with LPS for 3 h to induce inflammation. As shown in Figure 4A, the fluorescence imaging revealed an increase in fluorescence intensity over time when the inflamed MG-63 cells were incubated with the Fe$_3$O$_4$@Au-pep-CQDs nanoprobe. Notably, coincubation of the nanoprobe with an inhibitor for 4 h showed a distinct difference in fluorescence intensity compared to the group without the inhibitor, which underscores the specificity of the nanoprobe in detecting caspase-1. Further analysis of the fluorescence intensity of the image is depicted in Figure 4B.

Cytotoxicity assay of MG-63 cells and LO2 cells confirmed the minimal toxicity of the Fe$_3$O$_4$@Au-pep-CQDs nanoprobe (Figure S15) indicating their suitability for biological applications. The versatility of the Fe$_3$O$_4$@Au-pep-CQDs

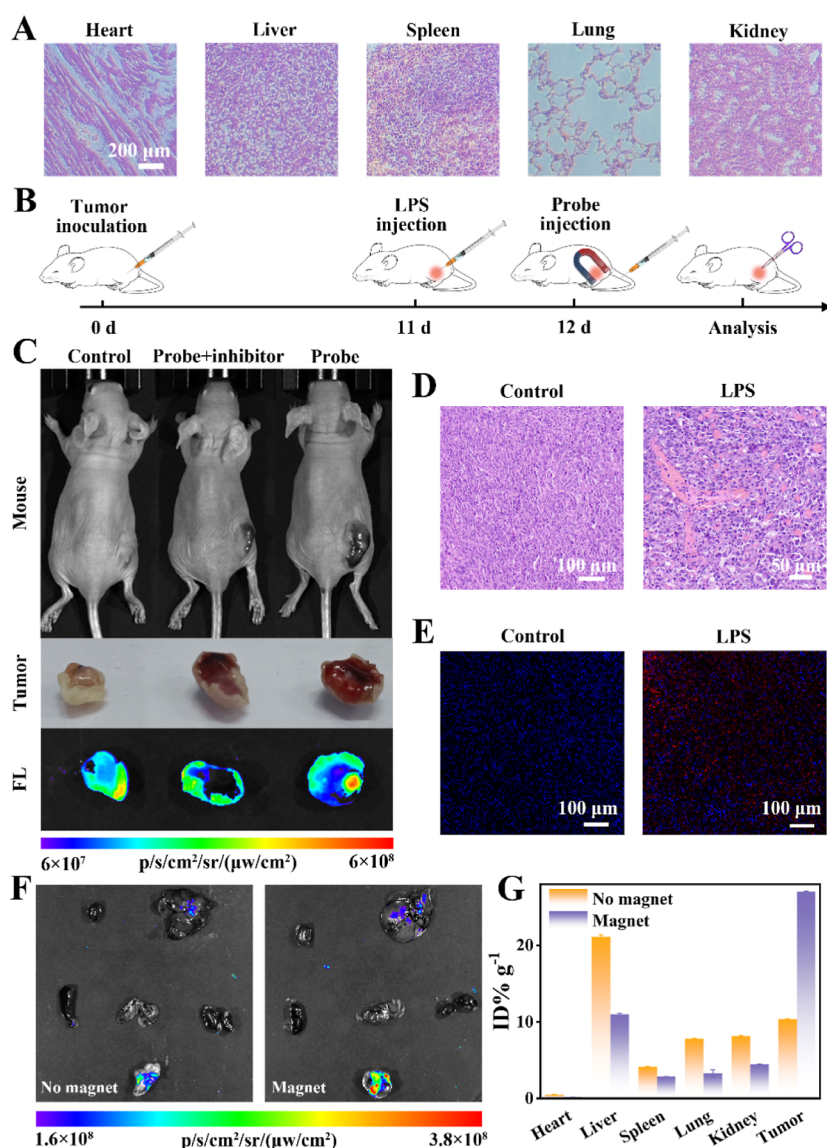**Figure 6.** (A) H&E staining of major organs after tail vein injection of Fe$_3$O$_4$@Au-pep-CQDs nanoprobe in MG-63 hormonal mice (×20 magnification). (B) Schematic diagram showing MG-63 mice model and in vivo experimental procedures. (C) Fluorescence imaging of dissected tumors in mice in the no-LPS-induced, LPS + inhibitor and LPS-induced groups. (D) H&E staining of tumor pathology sections (control: ×10 magnification, LPS: ×20 magnification). (E) Immunofluorescence of tumor sections (DAPI: nuclei, SpOrange: caspase-1) (×20 magnification). (F) Fluorescence imaging and (G) ICP−MS (Au elemental) analysis of major organs and tumors after Fe$_3$O$_4$@Au-pep-CQDs nanoprobe injection into MG-63-loaded mice (24 h after LPS injection at the tumor site).

nanoprobe was further examined across four different cell lines (control, 5 μg/mL LPS, 20 μg/mL LPS + inhibitor, and 20 μg/mL LPS groups). The changes in fluorescence intensity (Figure 4C,D) confirmed the applicability of the nanoprobe in caspase-1 detection across a broad range of cell types.

Cell migration and invasion assays, including scratch (Figure 5A,B) and Transwell (Figure 5C,D) assays, highlighted that inflammation could indeed promote tumor migration and invasion and exacerbate the condition in tumor patients. This highlights the importance of detecting inflammation in the tumor microenvironment.[32] The success of nanoprobes in 2D fluorescence activation in vitro prompted us to investigate their efficacy in 3D platforms. The 3D platform mimics the cellular microenvironment by facilitating cell−cell and cell−extracellular matrix interactions and can be used to simulate in vivo tumor tissue.[33−35] The 3D tumor cell model was constructed to simulate the inflammatory microenvironment in tumor

using LPS induction, and control, LPS + inhibitor, and LPS groups were established to explore the nanoprobe's potential in real tumor settings (Figure 5E,F). The fluorescence results showed that as the concentration of LPS increased, the fluorescence intensity of the cytospheres was higher. This proves that the higher the amount of caspase-1, the more severe the inflammation. Viability tests of LPS-induced 3D cells using the calcineurin-AM&PI staining method[36] demonstrated that cells incubated with 20 μg/mL LPS were still viable in large numbers. This reveals that the concentration of LPS used in the experiment can mimic the inflammatory environment of the tumor while still preserving cell proliferation.

In conclusion, the Fe$_3$O$_4$@Au-pep-CQDs nanoprobe is a promising tool for application in tumor cell imaging and is suited for widespread use in detecting caspase-1 within cells and cellular microenvironment.

In Vivo Imaging Applications of Fe₃O₄@Au-pep-CQDs Nanoprobe. To assess the suitability of nanoprobes in live animal models, we initially conducted a hemolysis experiment. The results (Figure S17) indicated that the hemolytic effect was negligible, confirming the nanoprobe is safe for in vivo experiments. Subsequent histological examination, which involved H&E staining of major organs 14 days postadministration of Fe₃O₄@Au-pep-CQDs nanoprobe via the tail vein in MG-63 tumor-bearing mice, was conducted (Figure 6A). The analysis revealed that there was no observable damage or inflammation in major organs. This shows that the Fe₃O₄@Au-pep-CQDs nanoprobe does not cause damage to major organs and is safe for bioapplications.

For targeted delivery, MG-63 nude mice, each with approximately 20 g, were used. Each mouse received an intratumoral injection with 0.15 mg LPS (per 20 g of body weight) to induce inflammation. After 24 h, 5 mg/mL of Fe₃O₄@Au-pep-CQDs nanoprobe was administered intravenously. A magnet was positioned at the tumor site to concentrate the nanoprobes,[37,38] and a local injection with a caspase-1 inhibitor was thereafter conducted. Tumors were excised at 6 h postinjection (Figure 6B). The tumors from the LPS-induced inflammation group exhibited clear signs of subcutaneous hemorrhage and erythema, whereas those from the control group tumors did not.[39] Fluorescence imaging (Figure 6C) confirmed higher fluorescence signals in tumors from the LPS group compared to those from the inhibitor-treated and non-LPS groups, suggesting the potential of nanoprobe for biopsy applications.

Further analysis involving H&E staining and immunofluorescence testing of tumor tissues from both LPS-induced and control mice was carried out. Under microscopic examination, the LPS group displayed distinct inflammatory foci with infiltrating inflammatory cells, and the cancer cells were visible.[40] In contrast, the control group did not exhibit inflammatory infiltration, but cancerous lesions with noticeable anisotropy were visible (Figure 6D).[41] Immunofluorescence staining using DAPI (nuclei) and SpOrange-labeled antibodies (caspase-1) highlighted the substantial caspase-1 activity in the LPS-induced tumors, in contrast to the control group, in which no fluorescent signals were detected (Figure 6E). This confirms the successful establishment of the mouse tumor inflammation model. Additionally, the experimental results obtained from the kit were consistent with those obtained from the Fe₃O₄@Au-pep-CQDs nanoprobe, which shows that the Fe₃O₄@Au-pep-CQDs nanoprobe has high potential in practical applications. Additional fluorescence imaging and ICP–MS analyses of major organs in mice with and without magnets demonstrated that magnetic targeting significantly enhanced the accumulation of Fe₃O₄@Au-pep-CQDs nanoprobe at the tumor site (Figure 6F,G). These findings validate the feasibility and practical applicability of Fe₃O₄@Au-pep-CQDs nanoprobe in targeted tumor imaging and inflammation detection in vivo.

CONCLUSION

In conclusion, we developed the "hedgehog ball"-shaped Fe₃O₄@Au-pep-CQDs nanoprobe as a novel solution for detecting inflammation at tumor sites. This advanced nanoprobe allows for simultaneous fluorescence and electrochemical detection and streamlines the analytical process by enhancing specificity and sensitivity through magnetic separation. This approach not only reduces the quenching of nanoparticles in

solution but also eliminates the need for frequent electrode changes. Our experiments confirmed that the Fe₃O₄@Au-pep-CQDs nanoprobe was highly effective in vitro and able to provide rapid and accurate biomarker analysis. The ability to conduct both FL and ECL detection using a single sample not only saves valuable biological material but also simplifies the diagnostic procedure, making it highly suitable for clinical settings. Moreover, inflammation associated with tumor sites can promote tumor progression through migration, invasion, and infiltration, which complicate the treatment while worsening patient outcomes. With its ability in the early detection of such inflammatory processes, our nanoprobe offers a significant advantage by potentially improving therapeutic strategies and patient care. Therefore, the Fe₃O₄@Au-pep-CQDs nanoprobe holds potential in various applications, including personalized medicine and targeted therapy.

■ ASSOCIATED CONTENT

ⓈI Supporting Information

The Supporting Information is available free of charge at https://pubs.acs.org/doi/10.1021/acs.analchem.4c03739.

> Additional experimental details, including materials and reagents, instruments, ECL efficiency of CQDs, ECL mechanism investigation of CDs/TEA system, cell culture, cell counting kit-8 (CCK-8) assay, establishment of mouse models, and supplementary figures, table and references (PDF)

■ AUTHOR INFORMATION

Corresponding Authors

Pinyi Ma — *College of Chemistry, Jilin Province Research Center for Engineering and Technology of Spectral Analytical Instruments, Jilin University, Changchun 130012, China;* ⓘ orcid.org/0000-0002-3230-4928; Email: mapinyi@jlu.edu.cn

Daqian Song — *College of Chemistry, Jilin Province Research Center for Engineering and Technology of Spectral Analytical Instruments, Jilin University, Changchun 130012, China;* ⓘ orcid.org/0000-0002-4866-1292; Email: songdq@jlu.edu.cn

Authors

Chen Zhao — *College of Chemistry, Jilin Province Research Center for Engineering and Technology of Spectral Analytical Instruments, Jilin University, Changchun 130012, China*

Mo Ma — *College of Chemistry, Jilin Province Research Center for Engineering and Technology of Spectral Analytical Instruments, Jilin University, Changchun 130012, China; School of Pharmacy, Jilin University, Changchun 130012, China*

Jukun Yang — *College of Chemistry, Jilin Province Research Center for Engineering and Technology of Spectral Analytical Instruments, Jilin University, Changchun 130012, China*

Zhuoxin Ye — *College of Chemistry, Jilin Province Research Center for Engineering and Technology of Spectral Analytical Instruments, Jilin University, Changchun 130012, China*

Complete contact information is available at:
https://pubs.acs.org/10.1021/acs.analchem.4c03739

Notes

The authors declare no competing financial interest.

ACKNOWLEDGMENTS

REFERENCES

(1) Coussens, L.; Zitvogel, L.; Palucka, A. *Science* **2013**, *339*, 286−291.

(2) Pribluda, A.; Elyada, E.; Wiener, Z.; Hamza, H.; Goldstein, R. E.; Biton, M.; Burstain, I.; Morgenstern, Y.; Brachya, G.; Billauer, H.; Biton, S.; Snir-Alkalay, I.; Vucic, D.; Schlereth, K.; Mernberger, M.; Stiewe, T.; Oren, M.; Alitalo, K.; Pikarsky, E.; Ben-Neriah, Y. *Cancer Cell* **2013**, *24*, 242−256.

(3) Jin, H.; Jin, X.; Zhang, H.; Wang, W. *Oncotarget* **2017**, *8*, 25571−25581.

(4) Jin, H.; Jin, X.; Cao, B.; Wang, W. *Oncol. Rep.* **2017**, *37*, 729−736.

(5) Fadare, O.; Bifulco, C.; Carter, D.; Parkash, V. *Mod. Pathol.* **2002**, *15*, 777−780.

(6) De Jong, M. M. E.; Chen, L. P.; Raaijmakers, M.; Cupedo, T. *Nat. Rev. Immunol.* **2024**, *24*, 543−558.

(7) Mantovani, A.; Allavena, P.; Sica, A.; Balkwill, F. *Nature* **2008**, *454*, 436−444.

(8) He, J.; Duan, P.; Liu, Y.; Feng, T.; Wang, S.; Lin, X.; Xie, J.; Liu, X. *Adv. Healthcare Mater.* **2024**, *13*, No. e2304439.

(9) Strowig, T.; Henao-Mejia, J.; Elinav, E.; Flavell, R. *Nature* **2012**, *481*, 278−286.

(10) Kolb, R.; Liu, G. H.; Janowski, A. M.; Sutterwala, F. S.; Zhang, W. Z. *Protein Cell* **2014**, *5*, 12−20.

(11) Di, Z.; Yi, X.; Li, L. *J. Am. Chem. Soc.* **2023**, *145*, 7931−7940.

(12) Yang, J. K.; Ma, M.; Wang, N. F.; Liu, L.; Zhao, C.; Li, J. K.; Chen, Y. X.; Ma, P. Y.; Song, D. Q. *Anal. Chem.* **2023**, *95*, 17654−17661.

(13) Liu, B.; Li, J.; Zhou, P.; Pan, W.; Li, N.; Tang, B. *Anal. Chem.* **2021**, *93*, 16880−16886.

(14) Liu, L.; Zhang, H.; Wang, Z.; Song, D. *Biosens. Bioelectron.* **2019**, *141*, 111403.

(15) Nandi, D.; Forster Iii, J.; Ramesh, A.; Nguyen, A.; Bharadwaj, H.; Kulkarni, A. *ACS Appl. Mater. Interfaces* **2023**, *15*, 55545−55558.

(16) Liu, L.; Chu, H.; Yang, J.; Sun, Y.; Ma, P.; Song, D. *Biosens. Bioelectron.* **2022**, *212*, 114389.

(17) Zu, F.; Yan, F.; Bai, Z.; Xu, J.; Wang, Y.; Huang, Y.; Zhou, X. *Microchim. Acta* **2017**, *184*, 1899−1914.

(18) Lin, Z.; Cheng, W.; Liu, C.; Zhao, M.; Ding, S.; Deng, Z. *Talanta* **2023**, *254*, 124101.

(19) Duff, D.; Baiker, A.; Edwards, P. P. *Langmuir* **1993**, *9*, 2301−2309.

(20) Li, F.; Yu, Z.; Zhao, L.; Xue, T. *RSC Adv.* **2016**, *6*, 10352−10357.

(21) Wang, G.-G.; Lv, Q.-Y.; Song, X.; Cui, H.-F. *Sens. Actuators B Chem.* **2021**, *344*, 130285.

(22) Marks, S.; Pinard, P.; Burgess, S.; Bithell, J.; Beanland, R. *Microsc. Microanal.* **2020**, *26*, 1212−1214.

(23) Zhang, J.; Werner, S.; Köppen, A.; Liu, X.; Shen, C.; Bertram, F.; Parak, W. J.; Sun, X. *Nano Today* **2024**, *57*, 102384.

(24) Wei, R.; Fu, G.; Li, Z.; Liu, Y.; Qi, L.; Liu, K.; Zhao, Z.; Xue, M. *J. Colloid Interface Sci.* **2024**, *663*, 644−655.

(25) Luo, J.; Li, T.; Yang, M. *Chin. Chem. Lett.* **2020**, *31*, 202−204.

(26) Gessner, I.; Park, J. H.; Lin, H. Y.; Lee, H.; Weissleder, R. *Adv. Healthcare Mater.* **2022**, *11*, No. e2102035.

(27) Chen, A.; Liang, W.; Wang, H.; Zhuo, Y.; Chai, Y.; Yuan, R. *Anal. Chem.* **2020**, *92*, 1379−1385.

(28) Guo, W.; Gao, X.; Zhan, R.; Zhao, Z.; Xu, K.; Tang, B. *Talanta* **2021**, *222*, 121525.

(29) Bolat, M.; Hatipoglu, H.; Koroglu, M.; Toptan, H.; Altindis, M. *World J. Microbiol. Biotechnol.* **2024**, *40*, 222.

(30) Hu, B.; Zhang, Q.; Gao, X.; Xu, K.; Tang, B. *Anal. Chem.* **2021**, *93*, 12022−12031.

(31) Bibo-Verdugo, B.; Salvesen, G. S. *Mol. Aspects Med.* **2022**, *88*, 101085.

(32) Zhang, X.; Li, C.; Chen, D.; He, X.; Zhao, Y.; Bao, L.; Wang, Q.; Zhou, J.; Xie, Y. H. *Inflamm. Res.* **2022**, *71*, 141−155.

(33) Distler, T.; Kretzschmar, L.; Schneidereit, D.; Girardo, S.; Goswami, R.; Friedrich, O.; Detsch, R.; Guck, J.; Boccaccini, A. R.; Budday, S. *Biomater. Sci.* **2021**, *9*, 3051−3068.

(34) Zhang, L.; Chen, K.; Zhang, H.; Pang, B.; Choi, C. H.; Mao, A. S.; Liao, H.; Utech, S.; Mooney, D. J.; Wang, H.; Weitz, D. A. *Small* **2018**, *14*, 1702955.

(35) Rainu, S.; Parameswaran, S.; Krishnakumar, S.; Singh, N. *J. Mater. Chem. B* **2022**, *10*, 5388−5401.

(36) Zhu, Y.; Xin, N.; Qiao, Z.; Chen, S.; Zeng, L.; Zhang, Y.; Wei, D.; Sun, J.; Fan, H. *ACS Appl. Mater. Interfaces* **2019**, *11*, 43018−43030.

(37) Wang, Y.; Pang, X.; Wang, J.; Cheng, Y.; Song, Y.; Sun, Q.; You, Q.; Tan, F.; Li, J.; Li, N. *J. Mater. Chem. B* **2018**, *6*, 2460−2473.

(38) Tang, X.; Manamanchaiyaporn, L.; Zhou, Q.; Huang, C.; Li, L.; Li, Z.; Wang, L.; Wang, J.; Ren, L.; Xu, T.; Yan, X.; Zheng, Y. *Small* **2022**, *18*, No. e2202848.

(39) Dudani, R.; Chapdelaine, Y.; van Faassen, H.; Smith, D. K.; Shen, H.; Krishnan, L.; Sad, S. *Infect. Immun.* **2002**, *70*, 1957−1964.

(40) Jialing, L.; Yangyang, G.; Jing, Z.; Xiaoyi, T.; Ping, W.; Liwei, S.; Simin, C. *Life Sci.* **2020**, *263*, 118587.

(41) Huang, R.; Ni, N.; Su, Y.; Gu, L.; Ju, Y.; Zhang, D.; Li, J.; Chang, M.; Chen, Y.; Gu, P.; Fan, X. *Chem. Eng. J.* **2024**, *479*, 147436.